Kinks, Nodal Bilayer Splitting, and Interband Scattering in $YBa_2Cu_3O_{6+x}$

S. V. Borisenko,[1] A. A. Kordyuk,[1,2] V. Zabolotnyy,[1] J. Geck,[1] D. Inosov,[1] A. Koitzsch,[1] J. Fink,[1] M. Knupfer,[1] B. Büchner,[1] V. Hinkov,[3] C. T. Lin,[3] B. Keimer,[3] T. Wolf,[4] S. G. Chiuzbăian,[5] L. Patthey,[5] and R. Follath[6]

[1]*IFW Dresden, P.O. Box 270116, D-01171 Dresden, Germany*
[2]*Institute of Metal Physics of National Academy of Sciences of Ukraine, 03142 Kyiv, Ukraine*
[3]*Max-Planck Institut für Festkörperforschung, D-70569 Stuttgart, Germany*
[4]*Forschungszentrum Karlsruhe GmbH, Institut für Festkörperphysik, D-76344 Karlsruhe, Germany*
[5]*Paul Scherrer Institut, CH-5232 Villigen PSI, Switzerland*
[6]*BESSY GmbH, Albert-Einstein-Strasse 15, 12489 Berlin, Germany*

(Received 24 November 2005; published 24 March 2006)

We apply the new-generation angle-resolved photoemission spectroscopy methodology to the most widely studied cuprate superconductor $YBa_2Cu_3O_{6+x}$. Considering the nodal direction, we found noticeable renormalization effects known as kinks both in the quasiparticle dispersion and scattering rate, the bilayer splitting, and evidence for strong interband scattering—all the characteristic features of the nodal quasiparticles detected earlier in $Bi_2Sr_2CaCu_2O_{8+\delta}$. The typical energy scale and the doping dependence of the kinks clearly point to their intimate relation with the spin-1 resonance seen in the neutron scattering experiments. Our findings strongly suggest a universality of the electron dynamics in the bilayer superconducting cuprates and a dominating role of the spin fluctuations in the formation of the quasiparticles along the nodal direction.

DOI: 10.1103/PhysRevLett.96.117004 PACS numbers: 74.25.Jb, 74.72.Bk, 79.60.−i

The presence of similar CuO planes in all high-temperature superconducting cuprates provides a key to understanding their puzzling generic phase diagram [1]. On the other hand, the sensitivity of the maximal transition temperatures (T_c) to the rest of the lattice implies that one should study the cuprates as a class of materials aiming to gain the knowledge of how to drive T_c. Because of the different purity of the samples, their mechanical properties, surface quality, size of the available single crystals, etc., a single experimental technique often provides information only about a few members of the large cuprate family. Angle-resolved photoemission spectroscopy (ARPES) has been successfully applied to many hole-doped cuprates. Although a hallmark of the modern ARPES is the sensitivity to the many-body effects and up to now only $Bi_2Sr_2CaCu_2O_{8+\delta}$ (BSCCO) and to a lesser degree $La_{2-x}Sr_xCuO_4$ (LSCO) turned out to be suitable targets for such studies. Investigations of $YBa_2Cu_3O_{6+x}$ (YBCO) by means of photoemission, despite a rich history [2], have been virtually stopped on the verge of the new millennium. In one of the last reports [3] the authors did find a single many-body related feature, the renown ''peak-dip-hump'' structure, but leave open some fundamental questions, such as the origin of the so called ''surface state'' and the presence of the bilayer splitting [4]. Thus, even the underlying band structure of YBCO, a basic prerequisite to study many-body interactions by ARPES, remains unclear [5].

In this Letter we extend the power of the new-generation ARPES to YBCO cuprates. Our first objective is the nodal direction which is known to be free of the influence of the surface state mentioned above [2,6]. We find not only a clear indication for the existence of the bilayer splitting but also other typical characteristics of the nodal quasiparticles found earlier in BSCCO and LSCO, such as dispersion anomalies dubbed ''kinks,'' their doping dependence, and a scattering rate at low energies consistent with the quadratic behavior. Remarkably, we also found evidence for the interband scattering which we have recently observed in a quite complicated experiment using circularly polarized light in BSCCO [7].

To ensure the generality of the observations, ARPES measurements were made on two different beam lines, the U125/1-PGM beam line at BESSY and the SIS beam line at the Swiss Light Source, using the same portable end station. Both beam lines deliver photons with comparable characteristics in terms of flux, resolution, and polarization in the energy range from 50 to 55 eV. The overall energy resolution was set to 12 meV, and the angular resolution to 0.2°. High-quality single crystals were synthesized by the solution-growth technique, annealed to the desired oxygen doping, and detwinned by a uniaxial mechanical stress at elevated T [8]. The samples thus obtained exhibit $T_c = 90$ K, $\Delta T_c < 1$ K, $T_c = 61$ K, $\Delta T_c < 2$ K, and $T_c = 35$ K, $\Delta T_c < 3$ K. In the following, we refer to the overdoped (OD) sample as OD90 and to the underdoped (UD) samples as UD61 and UD35, respectively.

A typical and essential component of the ARPES experiment is the possibility to select a suitable excitation photon energy. This advantage is illustrated in Fig. 1 where we show raw intensity maps taken along the nodal direction (right panel, inset) in the UD35 sample at 30 K as a function of photon energy. In agreement with local-density approximation (LDA) calculations [9], one observes two features corresponding to the bonding (B) and antibonding

 © 2006 The American Physical Society

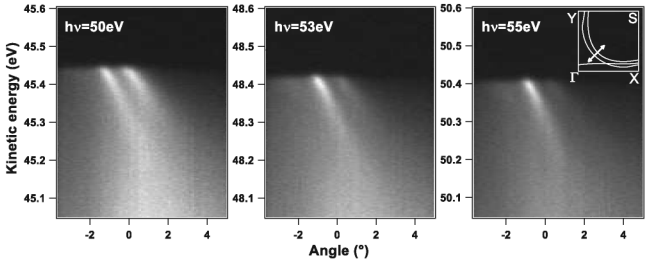

FIG. 1. Raw ARPES photoemission intensity measured using three different photon energies as a function of angle and kinetic energy of the photoelectrons. The inset schematically shows the LDA-predicted Fermi surface and a cut in the k space along which the data have been taken.

(A) components of the electronic structure of YBCO. Depending on the photon energy used, their intensity ratio changes, leading to the dominance of the bonding band at $h\nu = 55$ eV. This behavior is indeed expected as the similar change of the photon energy ($\sim$5 eV) resulted in significant variation of the bonding/antibonding intensity ratio in the case of BSCCO, where it was attributed to matrix element effects [10,11]. This similarity brings additional confidence that the two features shown in Fig. 1 are indeed bonding and antibonding states. Such a suppression of the antibonding band allows us to focus on the details of the bonding spectral distribution, knowing that we deal with a single feature.

In Fig. 2(a) we plot positions of the bonding momentum distribution curve's (MDC's) maxima as a function of energy. The deviation of this dispersion from the straight line passing through the Fermi momentum [dashed line in Fig. 2(a)], seen here to be significant already at $\sim$50 meV binding energy, is the famous kink detected before and well characterized in BSCCO and LSCO [5,12]. There, the origin of this feature is still controversial and its observation in a different cuprate can shed some light on this important issue. Upon closer consideration of the dispersion curve, we have noticed the presence of another, slightly less defined, kink at approximately 150 meV (gray arrow). This feature is less defined because the dispersion above and below this energy is not linear and the kink is seen only as a change of the curvature. The data shown in Fig. 2(b) confirm the presence of both features. Here the width of the MDC, which is directly proportional to the imaginary part of the self-energy (scattering rate), is plotted as a function of energy. As imaginary and real parts of the self-energy must be Kramers-Kronig related, one does expect that the characteristic features of one curve should reappear in the other. We can tentatively assign 70 and 180 meV binding energies to the two scattering rate kinks. Not only the presence of the kinks is reproduced in the scattering rate, but also the quadratic low energy behavior (dashed line in the right panel) agrees remarkably well with the linear dispersion near the Fermi level, clearly indicating the presence of quasiparticles [13]. In the insets we show a typical k_F energy distribution curve (EDC) and E_F MDC in order to illustrate our high resolution measurements.

Figure 3 represents a collection of data taken in the series of differently doped YBCO single crystals. An examination of the mass enhancement as a function of charge carrier concentration reveals a pronounced dependence of both low and high energy parts of the dispersion. To extract the kink energy, the low energy part of the data between E_F and some gradually increasing energy is fitted to a line passing through k_F. The high energy limit is then called a ''kink energy'' when the residuals start to sharply increase. As follows from the values given in Fig. 3, there is a clear energy shift of the kink to higher binding energies upon doping. This is in agreement with the previous studies on BSCCO [12,14,15] and LSCO [12], though the effect is more pronounced, most likely because of the clear separation between bilayer split components. We note that there exists also a systematic change of the Fermi velocity:

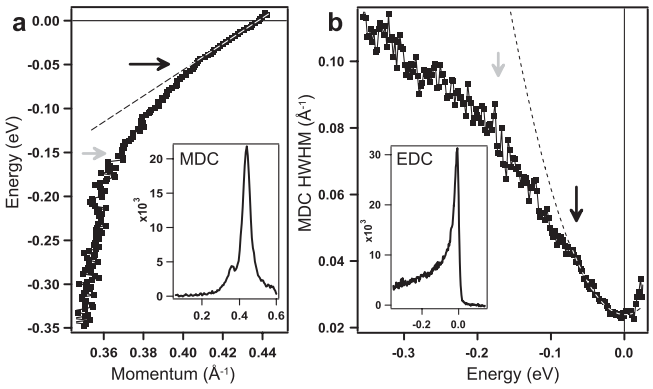

FIG. 2. Positions of the MDC's maxima (a) and their widths (b) as a function of binding energy for the UD35 sample. Dashed curves are fits to the low energy data. Black and gray arrows mark the energy positions of the low and high energy ''kinks,'' respectively. Insets show exemplary MDC and EDC.

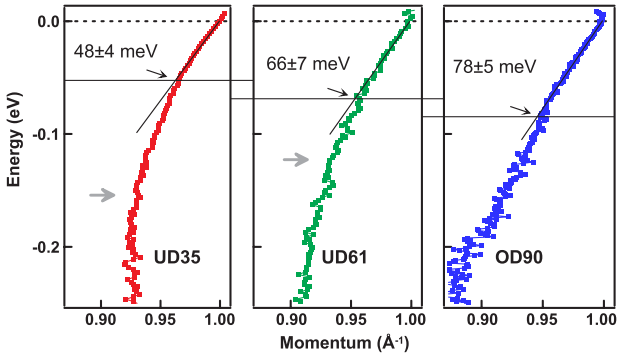

FIG. 3 (color online). Dispersion as a function of doping. Horizontal lines mark the energies of the kink, where dispersion starts to deviate from the straight line. Gray arrows show the position of the second high energy kink. Momentum scales are matched by putting $k_F = 1$ Å^{-1}.

1.47 eVÅ (UD35), 1.63 eVÅ (UD61), and 1.64 eVÅ (OD90).

Another familiar trend seen before in BSCCO [14] and LSCO [16] is the change of the high energy slope of the dispersion. Upon doping, it becomes less steep. The second kink, introduced in Fig. 2 for the UD35 sample, is visible also in the UD61 sample, but shifted to lower energy (~120 meV). If the energy of the second kink follows this trend further with doping, it is not surprising not to observe it in the slightly overdoped sample: most likely it merges with the upper one.

Tuning the excitation energy back to see both features, as in Fig. 1, we show in Figs. 4(a) and 4(b) dispersions corresponding to the A and B bands. The given values of the nodal bilayer splitting in momentum units are nearly 5 times larger than those in BSCCO [17], though comparable in differently doped samples. We take the opportunity to clearly distinguish between A and B bands to check another characteristic property of the near-nodal excitations in BSCCO—the recently observed strong interband scattering [7]. To recreate similar experimental conditions, we select a cut in the Brillouin zone which makes 10° with the nodal direction. The result is shown in Fig. 4(c). This time there was no need to use circularly polarized light to separate the bonding from the antibonding band. Already the raw data imply that the intensity distributions of the A and B features are different. MDCs taken at the Fermi level

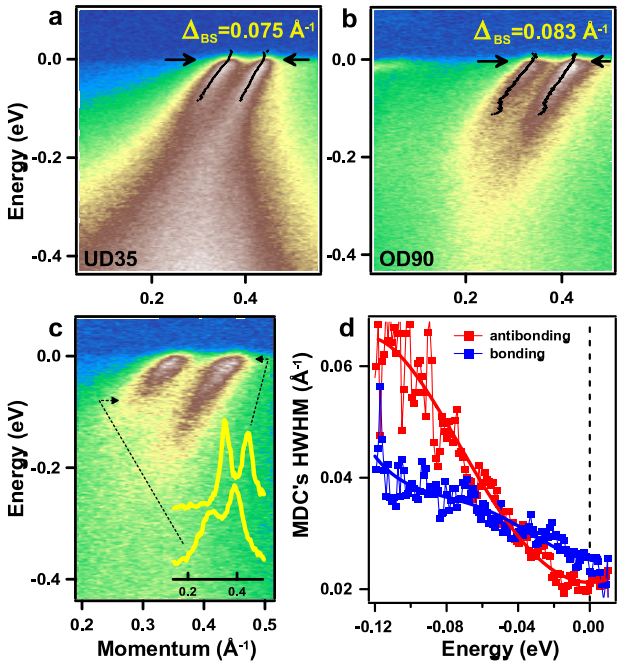

FIG. 4 (color online). (a),(b) Constancy of the nodal bilayer splitting. Solid lines are experimental dispersions. (c) Intensity map taken 10° away from the nodal direction in the OD90 sample. Solid yellow curves are the MDCs corresponding to the binding energies marked by black arrows. (d) Widths of the MDCs from panel (c).

and at 80 meV binding energy [solid yellow curves in Fig. 4(c)] both have a double-peak structure, but the relative intensity of the two components is significantly changing. This is a typical signature of the effect, since the intensity is inversely proportional to the imaginary part of the self-energy and thus to the scattering rate [7]. A more direct and important observation of the different scattering rates is presented in Fig. 4(d). We have fitted MDCs like those shown in Fig. 4(c) with two Lorentzians and plotted their widths as a function of binding energy. There is an unambiguous crossing of the two curves at ~50 meV making it qualitatively similar to the BSCCO case and thus indicating that the interband scattering suggested earlier to explain the effect [7] is plausible here also. The interband scattering means that the hole made in the antibonding band will most probably be filled by the "bonding" electron and vice versa. Within this scenario the difference in the scattering rates becomes natural: the densities of states (DOS) which correspond to the bonding and antibonding bands are different—both are peaked at the energies of the corresponding van Hove singularities. In the case of BSCCO, a simple estimate has shown that they cross at ~100 meV, exactly where the scattering rates are equal. The data from Fig. 4(d) are taken from the slightly overdoped sample where the antibonding band's van Hove singularity lies closer to the Fermi level. In addition, the bilayer splitting in YBCO is larger than in BSCCO. Therefore the crossover energy of ~50 meV perfectly fits the mentioned scenario.

Now we briefly overview the obtained results: (i) the nodal bilayer splitting is present in a series of differently doped $YBa_2Cu_3O_{6+x}$ single crystals and is virtually independent of x; (ii) the experimental dispersion of the bonding band exhibits a kink, which systematically shifts to higher binding energies upon increasing the hole concentration; (iii) there is another, less defined change of the curvature residing at higher energies which shifts towards the upper kink and probably merges with it already in the slightly overdoped sample; (iv) scattering rates which correspond to the bonding and antibonding bands are different being inversely proportional to the antibonding and bonding DOS, respectively. While result (i) is just a consequence of the underlying band structure predicted by LDA calculations [9], the other three are typical many-body effects detected for the first time in YBCO. We have shown earlier [18] that one can capture the main essentials of the electron dynamics along the nodal direction considering fermionic and bosonic channels of scattering. We implement this approach also here.

We believe that it is the fermionic channel that is responsible for the second elusive kink. The real part of the self-energy goes to zero at the energy related to the occupied bandwidth thus having a maximum at some lower energy which results in the kink [12]. As the occupied bandwidth decreases with doping, the second kink natu-

rally follows this trend. Another possible consequence of this behavior is that the high energy velocity then decreases since the bottom of the band slowly approaches the Fermi level. This effect is indeed observed here (Fig. 3) and earlier in BSCCO [14] and LSCO [16].

Results (ii) and (iv) can be understood in terms of the bosonic scattering channel. We do not repeat the arguments here as these features appear to be universal and have been discussed before in relation to BSCCO and LSCO [5,7]. What is controversial is the origin of the bosonic mode itself. The specificity of the present result is that the spectra are taken on exactly the same samples which have been studied by inelastic neutron scattering [8]. Thus, there is a unique opportunity to compare directly the typical energy scales of the charge and spin dynamics in the identical samples. As seen from Fig. 3, the energy of the kink monotonically increases with doping. This is exactly the property of the resonance peak [19] measured on the same single crystals [8,20]. The absolute energy of the kink does not match the energy of the resonance, and it actually should not as the resonance couples effectively only those regions on the Fermi surface which are separated by the momentum vector (π, π) or close to them. As is seen from Fig. 4(a), bonding nodal points in the UD35 sample are coupled by the vector $(0.77\pi, 0.77\pi)$, antibonding ones by $(0.65\pi, 0.65\pi)$, and bonding with antibonding ones by $(0.71\pi, 0.71\pi)$. According to recent experiments [21] and theoretical calculations [22] there is another resonance in the magnetic spectrum near the vector $(0.8\pi, 0.8\pi)$ at higher energies than the conventional (π, π) resonance. This new collective mode, being not fundamentally different from the resonant mode at (π, π), seems to track its doping dependence, thus perfectly supporting our observations. We do not think, however, that the nodal spectra can be fully explained in terms of a coupling to a single mode. The mentioned magnetic modes are rather sharp in momentum space. In reality the experimental dispersion always smoothly evolves in k space. It is also known that not only resonant parts of the magnetic excitation spectrum but also a spin-fluctuation continuum can be involved in the formation of the kinks [23]. It seems that more rigorous calculations which take into account full integration over the Fermi surface are needed to reproduce quantitatively the experiment. We believe that a phonon scenario is unlikely, as we are not aware of the existence of any phonon mode which scales with doping in such way.

The same is true for interband scattering. If our interpretation is correct, then the mediator of such scattering should have a corresponding symmetry. It is known that the magnetic excitations are dominant in the odd with respect to the layers exchange within a bilayer channel [24]. We are not aware of a similar property of any phonon mode which can couple nodal electrons. On the other hand, the emergence of interband scattering as a universal property of the cuprates can play a decisive role in the search for the mediator of such scattering and thus, perhaps, of the pairing. At present, a multitude of experimental facts led us to conclude that the spin fluctuations are the most likely candidates to mediate the pairing in cuprates.

In conclusion, our data provide a first observation of the kinks in both dispersion and scattering rate, as well as interband scattering, in a bilayer cuprate other than BSCCO. This implies a universality of these features which appear to be crucial for a complete understanding of high-temperature superconductivity.

The project is part of the Forschergruppe FOR538. This research project has been partially performed at the Swiss Light Source, Paul Scherrer Institut, Villigen, Switzerland, and has been supported by the European Commission under the 6th Framework Program through the Key Action: Strengthening the European Research Area, Research Infrastructures, Contract No. RII3-CT-2004-506008. We also thank R. Hübel for technical support.

[1] For example, J. L. Tallon and J. W. Loram, Physica (Amsterdam) **349C**, 53 (2001).
[2] B. W. Veal and Chun Gu, J. Electron Spectrosc. Relat. Phenom. **66**, 321 (1994); K. Gofron *et al.*, Phys. Rev. Lett. **73**, 3302 (1994); M. C. Schabel *et al.*, Phys. Rev. B **57**, 6090 (1998); **57**, 6107 (1998).
[3] D. H. Lu *et al.*, Phys. Rev. Lett. **86**, 4370 (2001).
[4] T. Yoshida *et al.*, Physica (Amsterdam) **351B**, 250 (2004).
[5] A. Damascelli, Z.-X. Shen, and Z. Hussain, Rev. Mod. Phys. **75**, 473 (2003).
[6] V. Zabolotnyy *et al.* (unpublished).
[7] S. V. Borisenko *et al.*, Phys. Rev. Lett. **96**, 067001 (2006).
[8] V. Hinkov *et al.*, Nature (London) **430**, 650 (2004).
[9] O. K. Andersen *et al.*, J. Phys. Chem. Solids **56**, 1573 (1995).
[10] A. A. Kordyuk *et al.*, Phys. Rev. Lett. **89**, 077003 (2002).
[11] S. V. Borisenko *et al.*, Phys. Rev. Lett. **90**, 207001 (2003).
[12] A. A. Kordyuk *et al.*, cond-mat/0510760.
[13] A. A. Kordyuk *et al.*, Phys. Rev. B **71**, 214513 (2005).
[14] P. D. Johnson *et al.*, Phys. Rev. Lett. **87**, 177007 (2001).
[15] A. D. Gromko *et al.*, Phys. Rev. B **68**, 174520 (2003).
[16] X. J. Zhou *et al.*, Nature (London) **423**, 398 (2003).
[17] A. A. Kordyuk *et al.*, Phys. Rev. B **70**, 214525 (2004).
[18] A. A. Kordyuk *et al.*, Phys. Rev. Lett. **92**, 257006 (2004).
[19] P. Bourges *et al.*, Science **288**, 1234 (2000); P. Dai *et al.*, Phys. Rev. B **63**, 054525 (2001); S. Pailhes *et al.*, Phys. Rev. Lett. **91**, 237002 (2003).
[20] V. Hinkov *et al.* (unpublished).
[21] S. Pailhes *et al.*, Phys. Rev. Lett. **93**, 167001 (2004).
[22] I. Eremin *et al.*, Phys. Rev. Lett. **94**, 147001 (2005).
[23] A. V. Chubukov and M. R. Norman, Phys. Rev. B **70**, 174505 (2004).
[24] H. F. Fong *et al.*, Phys. Rev. B **61**, 14 773 (2000).